11882 *Inorg. Chem.* **2009**, *48*, 11882–11888
DOI: 10.1021/ic901943e

Inorganic Chemistry
Article

The First Organic-Templated Vanadyl(IV) Gallophosphates with Ambient ^{51}V Hyperfine Structure, $\{V_2Ga_2O_{14}\}$ Cluster or Heterometal 12-Ring Channels

Li-Hsun Huang,[†] Yi-Chun Lai,[‡] Hui-Chun Lai,[†] Yun-Wei Chiang,[†] Jin-Hua Huang,[‡] and Sue-Lein Wang*,[†]

[†]*Department of Chemistry and* [‡]*Department of Materials Science and Engineering, National Tsing Hua University, Hsinchu 30013, Taiwan*

Received October 2, 2009

Three new vanadyl gallium phosphates, $(H_2dap)_3[(VO)_2(GaO)_2(PO_4)_4]\cdot H_2O$ (**1**), $(H_2dap)_{1.5}[(VO)_2(GaO)_2(PO_4)_3]\cdot 3H_2O$ (**2**), and $(H_2dap)[(VO)_2Ga_4(PO_4)_6(H_2O)_4]\cdot 2H_2O$ (**3**) (dap = 1,3-diaminopropane), have been prepared under mild solvothermal conditions and characterized by single-crystal X-ray diffraction, thermogravimetric analysis, magnetic susceptibility, and EPR spectroscopy. They are the first examples of an organic/V^{4+}/Ga/P/O system that displays three different dimensional structures with a common template. The 1D chain structure of **1** and the 2D layered **2** are both built up with a PO_4 and $\{V_2Ga_2O_{14}\}$ cluster which contains a *syn*-square pyramidal $\{V_2O_8\}$ dimer and two GaO_4 tetrahedra. The tetrameric cluster and V−O−Ga therein are observed in a metal phosphate system. Compound **3** is composed of $VO_5(H_2O)$ octahedra, $GaO_4(H_2O)$ trigonal bipyramids, and GaO_4 and PO_4 tetrahedra from which a unique 3D structure containing one-dimensional 12-ring channels is constructed. The channel aperture uncommonly comprises heterometal (V, Ga) polyhedra. Magnetic susceptibility data for **1**−**3** are consistent with V^{4+} and show a T_N of 12 K for **3**. The unusual *syn*-$\{V_2O_8\}$ dimers in **1** and **2** induce superexchange interactions, while isolated $VO_5(H_2O)$ octahedra in **3** display super-super-exchange interaction. Electron paramagnetic resonance spectra with ^{51}V hyperfine structures were distinctly observed at 300 K for **1**, while they started emerging at 30 K for **2** and 7 K for **3**. The average hyperfine constant, 85.56 Gauss, was obtained via spectral simulations and nonlinear least-squares fittings for **1** and **2**. Crystal data for **1** are triclinic, $P\bar{1}$, a = 9.1754(4) Å, b = 10.7853(5) Å, c = 15.6519(7) Å, α = 93.251(1)°, β = 92.530(1)°, γ = 95.106(1)°, V = 1538.4(1) Å^3, and Z = 2; for **2**, monoclinic, $P2_1/n$, a = 8.9195(3) Å, b = 14.6374(5) Å, c = 17.8608(6) Å, β = 97.272(1)°, V = 2313.1(1) Å^3, and Z = 4; and for **3**, monoclinic, $P2_1/c$, a = 9.0970(5) Å, b = 16.9940(9) Å, c = 9.6441(5) Å, β = 103.456(3)°, V = 1450.0(1) Å^3, and Z = 4.

Introduction

Since the discovery of cloverite in 1991,[1] exploitation of zeolitic materials has sparked an expansion to gallium phosphates/phosphites (GaPOs) with extra-large pores or channels. They potentially allow for research on host−guest reactions or the redox catalysis of large molecules as well as the generation of new topologies or properties.[2] Incorporation of transition metal ions into framework sites of aluminophosphates or gallophosphates is also of particular interest for the design of novel functional materials.[3] For example, the incorporation of manganese resulted in 3D chiral frameworks without using any chiral reagents,[3e] a low-T paramagnetic 3D structure,[3f] and mixed valency (Mn^{2+} and Mn^{3+}),[3g] and the incorporation of zinc led to production of the first 26-ring channel structure[3h] and nanoporous phosphate-based yellow/white LED phosphors.[3i] Directed by organic amine templates under mild hydrothermal conditions, many first-row transition metal ions such as $Ti^{3+/4+}$, V^{3+}, Cr^{3+}, $Mn^{2+/3+}$, $Fe^{2+/3+}$, Co^{2+}, Ni^{2+}, and Zn^{2+} have been successfully incorporated into the GaPO lattice to generate either isomorphous substituted[3j,4,5a] or unique MGaPO phases.[3e−i]

*To whom correspondence should be addressed. Fax: 886-35-711082. E-mail: slwang@mx.nthu.edu.tw.

(1) Estermann, M.; McCusker, L. B.; Baerlocher, C.; Merrouche, A.; Kessler, H. *Nature* **1991**, *352*, 320.

(2) (a) Bu, X.; Feng, P.; Stucky, G. D. *Science* **1997**, *278*, 2080. (b) Davis, M. E.; Saldarriaga, C.; Montes, C.; Garces, J.; Crowder, C. *Nature* **1988**, *331*, 698. (c) Sassoye, C.; Loiseau, T.; Faulelle, F.; Férey, G. *Chem. Commun.* **2000**, 943. (d) Guillou, N.; Gao, Q.; Forster, P. M.; Chang, J.; Nogues, M.; Park, S. E.; Férey, G. *Angew. Chem., Int. Ed.* **2001**, *40*, 2831. (e) Lin, C. H.; Wang, S. L.; Lii, K. H. *J. Am. Chem. Soc.* **2001**, *123*, 4649. (f) Férey, G. *Chem. Soc. Rev.* **2008**, *37*, 191. (g) Natarajan, S.; Mandal, S. *Angew. Chem., Int. Ed.* **2008**, *47*, 4798. (h) Yang, Y. C.; Chen, C. Y.; Wang, S. L. *J. Am. Chem. Soc.* **2008**, *130*, 1146. (i) Jhang, P. C.; Yang, Y. C.; Lai, Y. C.; Liu, W. R.; Wang, S. L. *Angew. Chem., Int. Ed.* **2009**, *48*, 742.

(3) (a) Hartmann, M.; Kevan, L. *Chem. Rev.* **1999**, *99*, 635. (b) Thomas, J. M.; Rafa, R.; Sankar, G.; Bell, R. G. *Nature* **1999**, *398*, 227. (c) Cowley, A. R.; Chippindale, A. M. *Chem. Commun.* **1996**, 673. (d) Feng, P. *Chem. Commun.* **2001**, 1668. (e) Lin, C. H.; Wang, S. L. *Chem. Mater.* **2002**, *14*, 96. (f) Hsu, K. F.; Wang, S. L. *Inorg. Chem.* **2000**, *8*, 1773. (g) Hsu, K. F.; Wang, S. L. *Chem. Commun.* **2000**, 135. (h) Lai, Y. L.; Lii, K. H.; Wang, S. L. *J. Am. Chem. Soc.* **2007**, *129*, 5350. (i) Liao, Y. C.; Lin, C. H.; Wang, S. L. *J. Am. Chem. Soc.* **2005**, *127*, 9986. (j) Lin, C. H.; Wang, S. L. *Inorg. Chem.* **2005**, *44*, 251.

(4) Lin, C. H.; Yang, Y. C.; Chen, C. Y.; Wang, S. L. *Chem. Mater.* **2006**, *18*, 2095.

 Published on Web 11/30/2009

There has been a large degree of interest in vanadium analogs of molecular sieves due to a high potential of catalyzing oxidation reactions. Additionally, we are interested in the search for new topologies and properties in vanadium-incorporated bimetal phosphates. According to a literature search, previously reported vanadium gallophosphates (VGaPOs) are rather limited, including only three organically templated V^{3+}-substituted gallophosphates,[5] two inorganic vanadyl(IV) gallophosphates,[6] and two organic−inorganic hybrid vanadyl(IV) gallium oxalatophosphates.[7] They were all synthesized with a V^{5+} source but resulted in reduced V^{3+}- or V^{4+}-containing products. Unlike Mn or Zn, the presence of V in the GaPO lattice merely led to isomorphous substitution (i.e., partial replacement of a Ga site) or isostructures. So far, unique structures of organically templated vanadyl(IV) gallophosphates have not been reported. In view of this, we simply started with V^{4+} reactants in the search for new VGaPOs and successfully prepared the first three V^{4+}-incorporated gallophosphates with a common organic template: $(H_2dap)_3[(VO)_2(GaO)_2(PO_4)_4]\cdot H_2O$ (**1**), $(H_2dap)_{1.5}[(VO)_2(GaO)_2(PO_4)_3]\cdot 3H_2O$ (**2**), and $(H_2dap)[(VO)_2Ga_4(PO_4)_6(H_2O)_4]\cdot 2H_2O$ (**3**) (dap = 1,3-diaminopropane). They all adopt new framework topologies exhibiting unique structural features unprecedented in metal phosphates. The paramagnetic V^{4+} ion in the structures of **1**−**3** were well characterized by diffraction, magnetic susceptibility, and spectroscopic methods. A magnetic structure study revealed superexchange of d^1 systems in **1** and **2** and super-super-exchange interaction in **3**. In contrast to the single-peak electron paramagnetic resonance (EPR) signal commonly observed for vanadyl(IV) phosphates, well-resolved hyperfine splittings resulting from coupling of d^1 electrons corresponding to the ^{51}V nucleus ($I = 7/2$) were surprisingly observed at ambient temperature for **1**, analogous to the diluted system of VO^{2+} doped into glass materials. The ^{51}V EPR hyperfine structure emerged at progressively decreasing temperatures with increasing dimensionality in the structures of **2** and **3**. In this paper, the synthesis, crystal structure, thermal analysis, magnetic property, and EPR study of the first three examples of the organic/V^{4+}/Ga/P/O system are described and discussed.

Experimental Section

Synthesis and Initial Characterization. All three compounds were synthesized under solvothermal reactions using 1,3-diaminopropane (dap) as a common organic structure-directing reagent. Other chemicals included $Ga(NO_3)_3$, $VOSO_4$, VO_2, 85% H_3PO_4, H_3PO_3, ethylene glycol (EG), and butanol. Chemicals of reagent grade were used as received. The starting reagents were heated in 23 mL Teflon-lined autoclaves under autogenous pressure at 160 °C for 3 days followed by slow cooling at 6 °C h^{-1} to room temperature. The products were filtered off, washed with water, rinsed with ethanol, and dried in desiccators at ambient temperature.

Single-phased dark-green chunky crystals of $(H_2dap)_3[(VO)_2(GaO)_2(PO_4)_4]\cdot H_2O$ (**1**) with yield of ∼60% (based on V) were obtained from a reaction mixture of dap (0.80 mL, 9.56 mmol), $Ga(NO_3)_3$ (0.256 g, 1 mmol), $VOSO_4$ (0.122 g, 0.75 mmol), and 85% H_3PO_4 (1.2 mL, 6 mmol) in a molar ratio of 9.56:1:0.75:6 in a mixed solvent of EG (4 mL) and water (8 mL) with an initial pH value of 9.21. By decreasing the amount of dap to 6 mmol (0.50 mL) and replacing H_3PO_4 with an equal amount (6 mmol) of H_3PO_3 in the above reaction (initial pH ∼ 6.30), greenish hexagonal plate-like crystals of $(H_2dap)_{1.5}[(VO)_2(GaO)_2(PO_4)_3]\cdot 3H_2O$ (**2**) were obtained as single-phase products with a yield of ∼53% (based on V). In the reaction for **3**, with a further decrease of dap to 3 mmol (0.25 mL) and a change of the V source to VO_2 (0.063 g, 0.75 mmol) with 6 mmol of H_3PO_4, a small amount of blue chunky crystals of $(H_2dap)[(VO)_2Ga_4(PO_4)_6(H_2O)_4]\cdot 2H_2O$ (**3**) appeared among two other phases.[8] The blue crystals of **3** were found to become a major product (only slightly contaminated with unknown turquoise powders) when the solvent system was modified to contain *n*-butanol (3.3 mL) and water (9 mL) (initial pH ∼ 2.53), wherein the other phases were completely suppressed. All three chemical formulas were primarily determined from single-crystal structure analysis (vide infra). The metal contents were confirmed by inductively coupled plasma−atomic emission spectrometry (ICP-AES); water and the organic contents were confirmed by TG and elemental analyses (EA). These measurements as well as magnetic susceptibility and EPR spectra were all performed on samples with individual purity carefully checked by powder X-ray diffraction (PXRD) patterns.

Single-Crystal X-Ray Diffraction Structure Analysis. Crystals of dimensions 0.15 × 0.15 × 0.30 mm for **1**, 0.10 × 0.15 × 0.30 mm for **2**, and 0.10 × 0.10 × 0.30 mm for **3** were selected for indexing and intensity data collections at 295 K for **1** and **3** and at 100 K for **2**. The measurements were performed on Bruker APEX diffractometer systems equipped with a sealed-tube X-ray source ($\lambda = 0.71073$ Å). Intensity data were collected in 2080 (for **1**), 1315 (for **2**), and 1271 (for **3**) frames with increasing ω (width of 0.3° per frame). Unit cell dimensions were determined by a least-squares fit of 4549 reflections for **1**, 5126 reflections for **2**, and 4446 reflections for **3**. The intensity data were corrected for Lp and absorption effects. Empirical absorption corrections based on symmetry-equivalent reflections were applied by using the SADABS program.[9] On the basis of systematic absences and statistics of intensity distribution, the space group was determined to be $P\bar{1}$ for **1**, $P2_1/n$ for **2**, and $P2_1/c$ for **3**. Direct methods were used to locate Ga, V, and a few oxygen atoms, with the remaining non-hydrogen atoms being found on difference maps. The template dap molecules plus hydrogen atoms were clearly observed on the Fourier difference maps in **1**, whereas they were disordered and could only be partially located on difference maps in **2** and **3**. On the basis of the results from bond-valence-sum (BVS) calculations,[10] the oxygen atoms O(21) in **1**; O(17), O(18), and O(19) in **2**; and O(16) in **3** were assigned to lattice water molecules, and O(13) and O(15) in **3** were assigned to coordinated water molecules. The final cycle of refinement, including the atomic coordinates, anisotropic thermal parameters for all non-hydrogen atoms, and fixed atomic coordinates and isotropic thermal parameters for H atoms, converged at $R_1 = 0.0259$ and $wR_2 = 0.0696$ for **1**, $R_1 = 0.0356$ and $wR_2 = 0.1016$ for **2**, and $R_1 = 0.0456$ and $wR_2 = 0.1026$ for **3**. Corrections for secondary extinction and anomalous dispersion were applied. Neutral-atom scattering factors for all atoms were taken from the standard sources. Calculations were performed on a PC using the SHELXTL-Plus programs.[11] Crystallographic data are listed in Table 1; selected bond lengths and ORTEP drawings with atomic labeling are given in the Supporting Information.

(5) (a) Chippindale, A. M. *Chem. Mater.* **2000**, *12*, 818. (b) Chippindale, A. M.; Peacock, K. J.; Cowley, A. R. *J. Solid State Chem.* **1999**, *145*, 379. (c) Chippindale, A. M.; Cowley, A. R. *J. Solid State Chem.* **2001**, *159*, 59.
(6) Hammond, R. P.; Zubieta, J. A. *J. Solid State Chem.* **1999**, *144*, 442.
(7) Chang, W. M.; Wang, S. L. *Chem. Mater.* **2005**, *17*, 74.
(8) The two phases included a known phase of $(H_2dap)(VO)_3(OH)_2(H_2O)_2(PO_4)_2$ (Soghomonian, V.; Chen, Q.; Haushalter, R. C.; Zubieta, J.; O'Connor, C. J.; Lee, Y. S. *Chem. Mater.* **1993**, *5*, 1690) and an unknown phase.
(9) Sheldrick, G. M. *SADABS*; Siemens Analytical X-ray Instrument Division: Madison, WI, 1998.
(10) Brown, I. D.; Altermatt, D. *Acta Crystallogr.* **1985**, *B41*, 244.
(11) Sheldrick, G. M. *Acta Crystallogr.* **2008**, *A64*, 112.

Table 1. Crystallographic Data for $(H_2dap)_3[(VO)_2(GaO)_2(PO_4)_4]\cdot H_2O$ (**1**), $(H_2dap)_{1.5}[(VO)_2(GaO)_2(PO_4)_3]\cdot 3H_2O$ (**2**), and $(H_2dap)[(VO)_2Ga_4(PO_4)_6(H_2O)_4]\cdot 2H_2O$ (**3**)

	1	**2**	**3**
chemical formula	$C_9H_{38}Ga_2N_6O_{21}P_4V_2$	$C_{4.5}H_{24}Ga_2N_3O_{19}P_3V_2$	$C_3H_{24}Ga_4N_2O_{32}P_6V_2$
fw	931.65	758.49	1166.82
space group	$P\bar{1}$ (No. 2)	$P2_1/n$ (No. 14)	$P2_1/c$ (No. 14)
a/Å	9.1754(4)	8.9195(3)	9.0970(5)
b/Å	10.7853(5)	14.6374(5)	16.9940(9)
c/Å	15.6519(7)	17.8608(6)	9.6441(5)
α/deg	93.251(1)	90	90
β/deg	92.530(1)	97.272(1)	103.456(3)
γ/deg	95.106 (1)	90	90
V/Å^3	1538.4(1)	2313.1 (1)	1450.0 (1)
Z	2	4	4
ρ_{calc}/g cm^{-3}	2.011	2.178	2.672
μ(Mo Kα)/mm^{-1}	2.622	3.385	4.743
T/°C	22	−173	22
λ(Mo Kα)/Å	0.71073	0.71073	0.71073
R_1[a]	0.0256	0.0356	0.0456
wR_2[b]	0.0696	0.1016	0.1026

[a] $R_1 = \sum||F_o| - |F_c||/\sum|F_o|$ for $F_o > 4\sigma(F_o)$. [b] $wR_2 = [\sum w(F_o^2 - F_c^2)^2/\sum w(F_o^2)^2]^{1/2}$, $w = [\sigma^2(F_o^2) + (aP)^2 + bP]^{-1}$, where a/b = 0.0414/0.00 for **1**, a/b = 0.0619/3.19 for **2**, and a/b = 0.0289/9.87 for **3** and $P = [\max(F_o)^2 + 2(F_c)^2)]/3$.

Thermal Study. Thermogravimetric analyses (TGA), using Perkin-Elmer TGA-7, were performed on the powder samples of **1** (3.11 mg), **2** (2.96 mg), and **3** (3.29 mg) under flowing N_2 with a heating rate of 10 °C min^{-1}. TG curves of all samples (Figure S1, Supporting Information) showed a common feature of immediate weight loss beginning at 50 °C, corresponding to the removal of lattice water. As indicated in the TG curve of **1**, the first observed weight loss (~2.0%) before 170 °C should correspond to the evacuation of lattice water molecules (ca. 1.9% for H_2O). According to the TG curves of **2** and **3**, complete removal of the lattice water molecules should occur at ca. 250 °C for **2** ($3H_2O$, ca. 7.1%) and ca. 110 °C for **3** ($2H_2O$, ca. 3.1%). Besides lattice water, the first stage of weight loss in the TG curve of **3** also involved partial removal of the coordination waters (ca. > $3H_2O$). All TG curves showed unresolved multistage weight losses beyond 250 or 300 °C, attributed to the decomposition and dehydration of organic templates. The total observed weight loss, 29.8% for **1**, 24.4% for **2**, and 17.1% for **3**, can be compared well with the calculated 31.6% ($4H_2O$ + 3dap) for **1**, 25.3% ($4.5H_2O$ + 1.5dap) for **2**, and 17.1% ($7H_2O$ + 1dap) for **3**.

Magnetic Susceptibility and EPR Study. Variable-temperature magnetic susceptibility $\chi(T)$ was measured from 2 to 300 K in a magnetic field of 5 kG using a SQUID magnetometer on powder samples of **1** (33.7 mg), **2** (30.7 mg), and **3** (15.6 mg). Corrections for diamagnetic contribution were made according to Selwood.[12] The magnetic data in the form of χ_M versus T, $\chi_M T$ versus T, and χ_M^{-1} versus T were analyzed and fitted on the basis of Curie−Weiss behavior: $\chi_M = C/(T-\theta)$. Curie constant (C in cm^3 K mol^{-1}) and Weiss temperatures were respectively obtained: C = 0.610 and θ = −34.3 K for **1**, C = 0.748 and θ = −96.5 K for **2**, and C = 0.699 and θ = −6.1 K for **3**. The effective moments (μ_{eff}) per formula (2 V^{4+}) obtained for **1**−**3** were respectively 2.21, 2.45, and 2.36 μ_B, which compared well with the spin-only value, 2.45 μ_B. X-band EPR spectra were recorded with a Bruker EMX-10 spectrometer between 4 and 300 K. The g values of these signals were measured relative to DPPH (g = 2.0036). Spectral simulations and nonlinear least-squares fittings for the hyperfine structures of **1** and **2** were performed using MATLAB with the EasySpin toolbox.[13] The Nelder-Mead simplex algorithm was used for numerical optimizations. The optimal magnetic tensors obtained and used were g = (1.967, 1.990, 1.944) and A = (17.016, 60.585, 179.091) Gauss, giving an average hyperfine constant A_0 = 85.564 Gauss.

(12) Selwood, P. W. *Magnetochemistry*; Interscience: New York, 1956.
(13) Stoll, S.; Schweiger, A. *J. Magn. Reson.* **2006**, *178*, 42.

Results and Discussion

Description and Relations of Structures. Compounds **1**−**3** adopt three unique structures with the inorganic frameworks containing crystallographically independent tetra-valent vanadium centers with four-membered rings (4Rs) of gallophosphate in common (Figures 1−3). All showed typical vanadyl (V=O) bonds with distances ranging from 1.602(2) to 1.627(2) Å, and the +4 oxidation state of V has been confirmed by BVS calculations and a magnetic study. The three VGaPO frameworks with three varied dimensions but templated by an identical organic cation, H_2dap^{2+}, are a rare case in extended structures. According to a literature search, diprotonated dap molecules were reported in vanadium phosphates with a 3D structure only.[14] It is noticeable that the H_2dap^{2+} ions are most densely packed in **1**, which is observed to decrease with increasing structural dimensions from **1** to **3**. The same trend was observed in the smaller ethylene diamine-templated vanadium phosphate system as well.[15] Such diamine molecules seem highly flexible in directing multi-dimensional structures.

Compound **1** adopts a 1D chain structure which is built up with two independent VO_5 square pyramids, two GaO_4 and four PO_4 tetrahedra, and three moieties of H_2dap^{2+}. The two VO_5 square pyramids share a common edge forming a dimeric unit that displays a relatively rare *syn* configuration of vanadyl groups compared to the commonly observed *anti* configuration in vanadium phosphates.[16] As depicted in Figure 1a, the skeleton of the chain is built from alternating *syn*-$\{V_2O_8\}$ dimers and 4Rs of $GaPO_4$ with inversion centers located in the centers of 4Rs. Within the chains, an unprecedented heterotetramer unit of $\{V_2Ga_2O_{14}\}$ is located, which is an assembly of one *syn*-$\{V_2O_8\}$ dimer and two GaO_4 tetrahedra connected on the common

(14) (a) Loiseau, T.; Férey, G. *J. Solid State Chem.* **1994**, *111*, 416. (b) Soghomonian, V.; Chen, Q.; Haushalter, R. C.; Zubieta, J. *Chem. Mater.* **1993**, *5*, 1595.
(15) Murugavel, R.; Choudhury, A.; Walawalkar, M. G.; Pothiraja, R.; Rao, C. N. R. *Chem. Rev.* **2008**, *108*, 3549.
(16) (a) Zhao, Y.; Shi, Z.; Ding, S.; Bai, N.; Liu, W.; Zou, Y.; Zhu, G.; Zhang, P.; Mai, Z.; Pang, W. *Chem. Mater.* **2000**, *12*, 2550. (b) Yang, Y. C.; Hung, L. I.; Wang, S. L. *Chem. Mater.* **2005**, *17*, 2833.

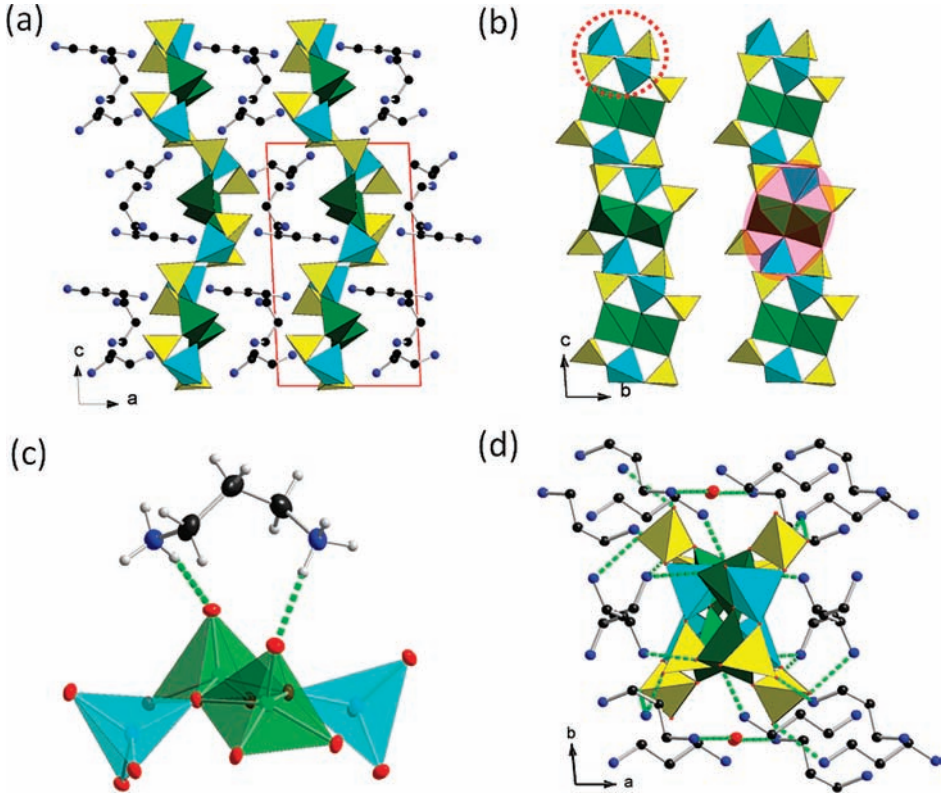

Figure 1. Polyhedral representation of structure **1**. (a) Projection along *b* showing 1D chains templated by H_2dap^{2+} ions. (b) Section of chains containing *syn*-$\{V_2O_8\}$ dimer (green), 4R of $GaPO_4$ (in dotted circle, cyan tetrahedra for Ga and yellow for P), and $\{V_2Ga_2O_{14}\}$ heterotetramer (in shaded oval circle). (c) Side view of tetramer showing hydrogen bonds (green dashed lines) to one H_2dap^{2+} ion. (d) Perspective view of a 1D chain showing hydrogen-bonded network.

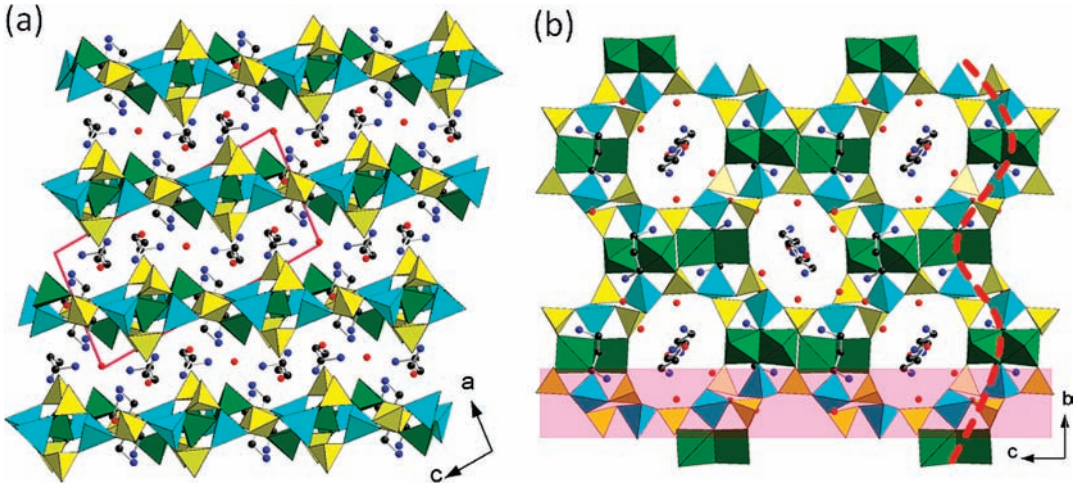

Figure 2. Polyhedral plots of the layered structure **2**. (a) Perspective view along the *b* axis showing interlayer H_2dap^{2+} ions (in ball-and-stick model) and lattice water (red solid circles). (b) Section of a single layer showing wavy chains, 4R chains (in rectangular shaded region), and 12R windows.

edge (Figure 1b), resulting in a $V^{4+}-O-Ga$ linkage first observed in microporous materials. As depicted in Figure 1c, each *syn* dimer is capped with one H_2dap^{2+} ion via two hydrogen bonds. Noticeably, the four unique PO_4 tetrahedra in **1** are found in two coordination modes: the two connected to two Ga and one V polyhedra are in the η^3 mode, whereas the other two connected to one Ga and one V polyhedra are in the η^2 mode. Each $\{V_2Ga_2O_{14}\}$ unit is capped by two η^2-PO_4 tetrahedra pendent on both sides of the linear chain. The neighboring $\{V_2Ga_2O_{14}\}$ clusters within an individual chain are inversion-related and linked by η^3-PO_4 tetrahedra. Unlike hydrogen phosphate groups, orthophosphate tetrahedra are scarcely found to act as terminal pendent groups.[17] Stabilization of the η^2-PO_4 groups in **1** is presumably supported by the abundant hydrogen bonds from H_2dap^{2+} ions (Figure 1d), which completely surround and fill in the space between the square-packing chains.

(17) Lii, K. H.; Huang, Y. F.; Zima, V.; Huang, C. Y.; Lin, H. M.; Jiang, Y. C.; Liao, F. L.; Wang, S. L. *Chem. Mater.* **1998**, *10*, 2599.

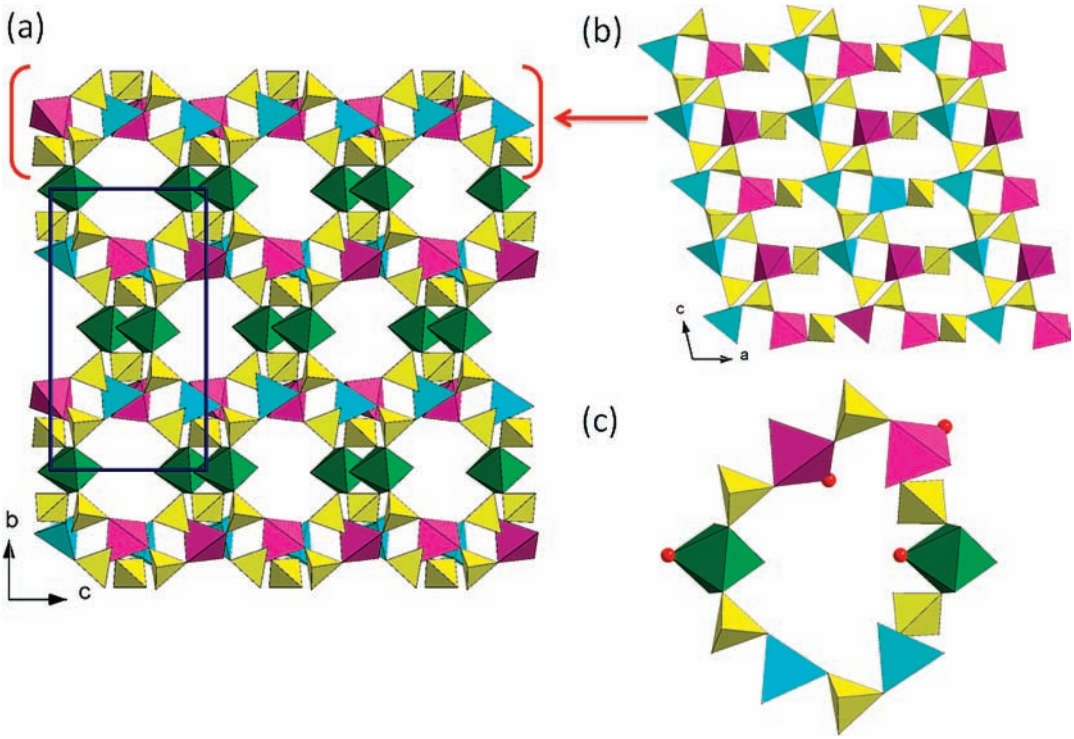

Figure 3. Structure of **3**. Projection along *a* showing that the 3D inorganic framework (a) is composed of gallium phosphate [$4^2 8^2 + 4^2 8^1 + 8^2$] sheets (b) and isolated $VO_5(H_2O)$ octahedra. The heterometal 12R window of extra-large channels surrounded by two $VO_5(H_2O)$ octahedra, two $GaO_4(H_2O)$ TBPs, two GaO_4, and six PO_4 tetrahedra is shown in (c).

Compound **2** possesses the same structural building units as compound **1**, but they lead to a two-dimensional layer structure instead. In **2**, the coordination modes of phosphate groups were found raised to η^4 and η^3 (Figure 2). Similar to **1**, each $\{V_2Ga_2O_{14}\}$ cluster is connected to the other two clusters through two η^3-PO_4 groups, forming wavy infinite chains along *b* (Figure 2b). These wavy chains hold no pendent PO_4 groups and no inversion symmetry like the linear chains of **1**. In addition, two neighboring $\{V_2Ga_2O_{14}\}$ clusters on adjacent wavy chains are connected via η^4-PO_4 tetrahedra, which are absent in compound **1**. Consequently, compound **2** possesses a layer composition with one PO_4 less in comparison to **1**. Also shown in Figure 2b is that the layer may be alternatively viewed as gallophosphate chains (consisting of $GaPO_4$ 4Rs and η^4-PO_4 running parallel to *c*) connected by *syn*-$\{V_2O_8\}$ dimers on the *bc* plane. Between either the wavy chains or the 4R + η^4-PO_4 chains, the 12-ring channel along *a* with a heterometal opening composed by two VO_5, $4GaO_4$, and $6PO_4$ polyhedra with a maximum free diameter of 7.49 Å, taking into account the van der Waals radius of oxygen atoms (1.35 Å), can be observed. Two-thirds of the lattice water molecules and one-third of the disordered H_2dap^{2+} ions were located within layers in the 12Rs. The remaining counterspecies were located in the interlayer space where the H_2dap^{2+} ions are less disordered so that some hydrogen bonds to η^3-PO_4 groups were allowed to be detected.

Dissimilar to **1** and **2**, compound **3** contains $VO_5(H_2O)$ octahedra, $GaO_4(H_2O)$ trigonal bipyramids (TBPs), and GaO_4 and η^4-PO_4 tetrahedra. The 4R chains formed by one TBP of Ga and tetrahedra of Ga and P running parallel to *c* can be observed to connect into [$4^2 8^2 + 4^2 8^1 + 8^2$] sheets via additional PO_4 tetrahedra on the *ac* plane (Figure 3). Unlike VO_5 in the dimer unit of **1** and **2**, the isolated $VO_5(H_2O)$ octahedra bridge between the gallophosphate sheets to create a unique 3D open network with extra-large channels running along *a*. The channels have an opening surrounded by 12 polyhedra of $2VO_5(H_2O)$, $2GaO_4(H_2O)$, $2GaO_4$, and $6PO_4$ with a maximum free diameter of 8.29 Å, taking into account the van der Waals radius of oxygen atoms (1.35 Å). The heterometal 12-ring channel with three kinds of mixed M−O polyhedra has not been observed in metal phosphates. The coordination water molecules of $VO_5(H_2O)$ are all pointing toward the channel space and forming hydrogen bonds with lattice waters, which together with H_2dap^{2+} reside within channels.

Structure-Related Properties. Despite its lowest dimensionality, the structure of **1** showed better thermal stability than the higher-dimensional **2**. The highly densely packed H_2dap^{2+} moiety around every infinite VGaPO chain allowed six strong hydrogen bonds per H_2dap^{2+} ion to either oxygen atoms on the vanadyl or phosphate groups (Figure 1d). As a consequence, a rigid hydrogen-bonded 3D network is constructed for **1**. In contrast, disordered H_2dap^{2+} ions in **2** are not able to form presentable hydrogen bonds to enhance rigidity of the structure. Indeed, the framework of **2** would immediately collapse by dehydration; it even became amorphous by standing under ambient conditions after weeks. Among them, compound **3** is unsurprisingly the most stable one. On the basis of the combined results of TGA and PXRD measurements, we confirmed that the framework of **3** could sustain the removal of lattice water and even some coordination water molecules, a feature worth noting of transition metal incorporated GaPOs.[3e] The rest of the coordination water should be an indispensable part of the

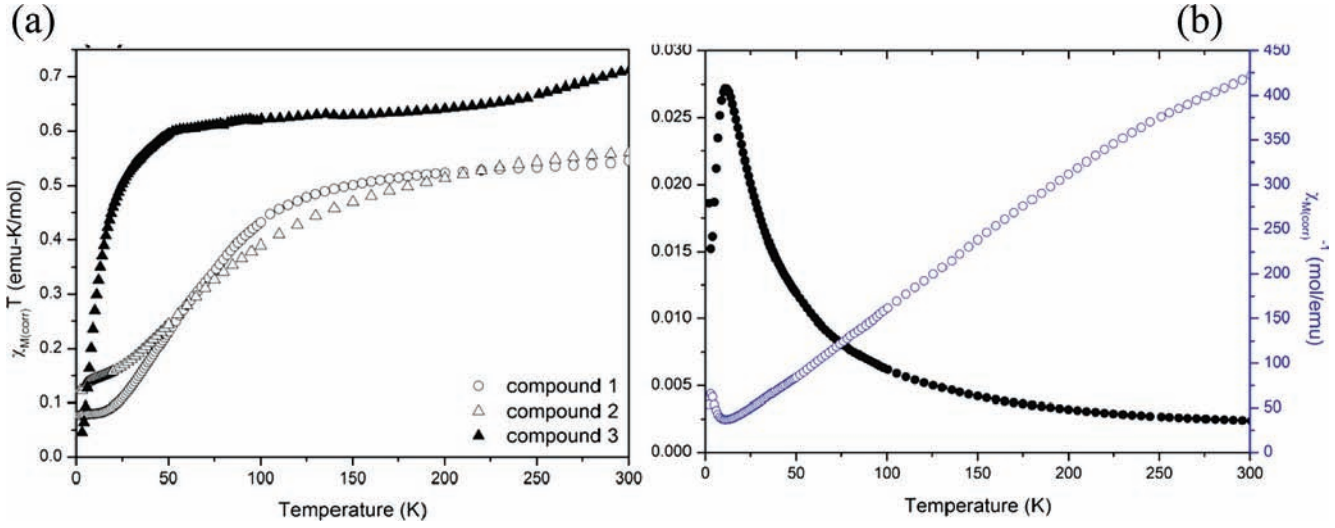

Figure 4. (a) $\chi_M T$ versus T curve for all three compounds, indicating antiferromagnetic behavior for compounds **1**−**3** (b) Susceptibility versus T curves for **3** showing T_N at 12 K (● for χ_M versus T and ○ for χ_M^{-1} versus T).

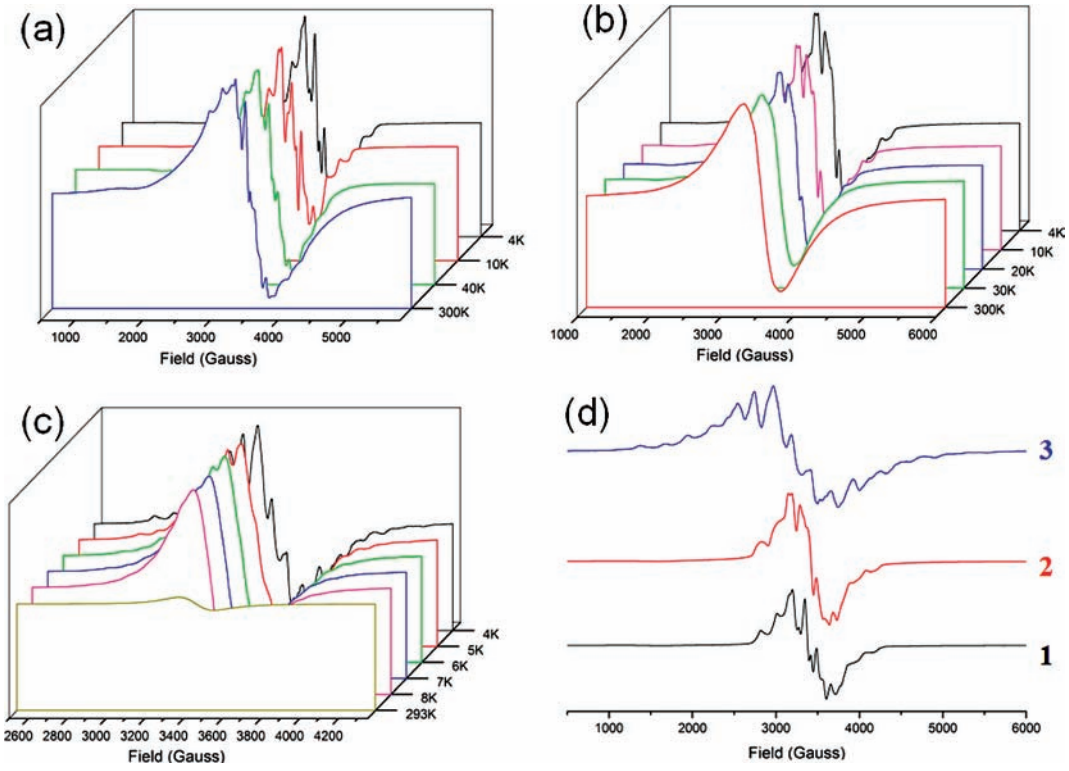

Figure 5. Powder EPR spectra of **1**−**3**. (a) Spectra of **1** measured at 300 K, 40 K, 10 K, and 4 K. (b) Spectra of **2** at 300 K, 30 K, 20 K, 10 K, and 4 K. (c) Spectra of **3** at 293 K and 8−4 K. (d) Spectra measured at 4 K showing relative hyperfine splitting observed for the three compounds.

framework, since it was confirmed that the structure will no longer be retained after complete removal of them.

All three compounds are d^1 systems showing typical paramagnetism at room temperature and antiferromagnetism (AFM) at low temperatures. As observed in $\chi_M T$ versus T curves (Figure 4b), the low-dimensional **1** and **2** became AFM below 100 K, whereas the higher-dimensional **3** did so below 50 K. The large negative Weiss constants for **1** and **2** confirmed the AFM. Additionally, Goodenough−Kanamori−Anderson rules[18] were applied to better understand their magnetic structures. With the $\{V_2O_8\}$ dimers in the *syn* configuration and the distance between two V centers (3.02 Å) short enough, super-exchange mechanisms are accordingly expected to lead to antiferromagnetic interactions in **1** and **2**. In the structure of **3**, the isolated V^{4+} ions, which are connected by PO_4 tetrahedra and at a closest distance of 5.157 Å, could enable super-super-exchange interactions through V−O···O−V. The V−O···O angles, 125.9° and 131.6°, are all greater than 120°, indicating antiferromagnetic interaction is more favorable. We observed a maximum in

(18) Goodenough, J. B. *Magnetism and the Chemical Bond*; Interscience: New York, 1963.

the plot of χ_M versus T at 12 K, revealing that 3D magnetic ordering was readily achieved in the isolated d^1 system of **3**.

As observed in powder EPR spectra (Figure 5), all three compounds exhibit hyperfine splitting peaks, from an ambient temperature for **1**, 30 K for **2**, and 7 K for **3**, which are rather uncommon for pure compounds except doped materials. The temperature for emerging hyperfine splitting as a function of temperature can be used to probe low-concentration paramagnetic species.[19] The V^{4+} centers in compounds **1**−**3** seem to be "diluted" by Ga/P/O matrices, inducing unique EPR spectra first observed in pure vanadyl phosphates but in amorphous glass with low concentrations of doped VO^{2+}.[20] To better understand the intriguing dipole−dipole coupling of electron spins and coupling of electron and nucleus-spin interactions of the V^{4+} centers in the *syn*-$\{V_2O_8\}$ dimers residing in $\{V_2Ga_2O_{14}\}$ clusters, the 4 K spectra of compound **1** and **2** were fitted with the spectra simulated at the presence of strong exchange J coupling whose corresponding Pake pattern is obtained in the deconvolution analysis using the Tikhonov method. The J integrals extracted from the deconvoluted Pake patterns are 130 Gauss for **1** and 174 Gauss for **2**. The J-coupling effect in compound **2** is indeed stronger than that in **1**, consistent with inter- and intrainteractions between $\{V_2O_8\}$ dimers in **1** and **2**. Different extents of dipole−dipole coupling were reflected in the hyperfine structure at 4 K (Figure 5d): the splitting peaks of the spectrum for **1** are more distinct than the spectrum for **2** as a stronger dipole−dipole interaction increases the line width and lowers the resolution of the spectra. The average hyperfine constant, 85.56 Gauss, was obtained via spectral simulations and nonlinear least-squares fittings for **1** and **2**. The interspin distance derived from the EPR data, 3.20 Å for **1** and 3.31 Å for **2**, could be compared with the V···V distances revealed by crystallographic analysis for *syn*-$\{V_2O_8\}$ dimers: 3.03 Å for **1** and 3.02 Å for **2**.

Conclusion

In this study, we have succeeded in obtaining three new materials of V^{4+}-incorporated gallophosphates by employing a V^{4+} chemical under mild solvothermal conditions. All three compounds adopt new framework topologies exhibiting unique structural features unprecedented in metal phosphates. The framework topologies exhibit unique features of the $\{V_2Ga_2O_{14}\}$ cluster unit containing *syn*-square pyramidal $\{V_2O_8\}$ dimers, a V−O−Ga linkage, or 12-ring heterometal (V, Ga) channels rarely observed in the metal phosphate system. The common template of H_2dap^{2+} seems to play an important role in determining the relative stability of varied structures through hydrogen-bonding interactions particularly with vanadyl groups. All three compounds with embedded tetravalent vanadium show paramagnetism at room temperature and antiferromagnetism at low temperatures. The V^{4+} centers in compounds **1**−**3** seem to be "diluted" by a Ga/P/O matrix, as these materials could display hyperfine structures detectable at high temperatures, 300 K for **1**, 30 K for **2**, and 7 K for **3**. The hyperfine splitting arises at ambient temperature for **1** and is unprecedented for pure vanadyl(IV) phosphates, except the diluted system of VO^{2+}-doped materials. The pursuit of more new structures with extra-large channels or new properties in the organic/V/Ga/P/O system is in progress.

Acknowledgment. We are grateful to the National Science Council of Taiwan for support of this work (97-2113-M-007-013-MY3).

Supporting Information Available: X-ray crystallographic information files (CIF), tables of ICP-AES and EA analyses, ORTEP drawings, structure plots, as-measured and simulated powder patterns for **1** and **2**, variable-temperature powder XRD patterns for **3**, and susceptibility (χ_M) versus T. This material is available free of charge via the Internet at http://pubs.acs.org.

(19) (a) Shpeizer, B. G.; Xiang, O.; Heising, J. M.; Clearfield, A. *Chem. Mater*. **2001**, *13*, 2288. (b) Shvareva, T. Y.; Beitz, J. V.; Duin, E. C.; Albrecht-Schmitt, T. E. *Chem. Mater*. **2005**, *17*, 6219. (c) Rojo, J. M.; Mesa, J. L.; Calvo, R.; Lezama, L.; Olazcuaga, R.; Rojo, T. *J. Mater. Chem*. **1998**, *8*, 1423.

(20) (a) Agarwal, A.; Seth, V. P.; Gahlot, P. S.; Khasa, S.; Chand, P. *Mater. Chem. Phys*. **2004**, *85*, 215. (b) Kumar, V. R.; Chakradhar, R. P. S.; Murali, A.; Gopal, N. O.; Rao, J. L. *Int. J. Mod. Phys. B* **2003**, *17*, 3033. (c) Agarwal, A.; Seth, V. P.; Gahlot, P. S.; Khasa, S.; Chand, P. *J. Phys. Chem. Solids* **2003**, *64*, 2281. (d) Poonguzhali, R.; Venkatesan, R.; Rajendiran, T. M.; Rao, P. S.; Ravikumar, R. V. S. S. N.; Reddy, Y. P. *Cryst. Res. Technol*. **2000**, *35*, 10.